High-pressure synthesis of heavily hole-doped cuprates $Mg_{1-x}Li_xCu_2O_3$ with quasi-one-dimensional structure

Yoshinori Imai,[1,*] Koya Sasaki,[1] Takuya Aoyama,[1] Kenji Shirasaki,[2] Tomoo Yamamura,[2,3] and Kenya Ohgushi[1]

[1]*Department of Physics, Graduate School of Science, Tohoku University, 6-3 Aramaki-Aoba, Aoba-ku, Sendai, Miyagi 980-8578, Japan*

[2]*Institute for Materials Research, Tohoku University, Sendai, Miyagi 980-8577, Japan*

[3]*Institute for Integrated Radiation and Nuclear Science, Kyoto University, Kumatori-cho, Osaka 590-0494, Japan*

(Received 21 November 2019; revised manuscript received 20 May 2020; accepted 21 May 2020; published 2 June 2020)

We investigate electronic properties of hole-doped cuprates $Mg_{1-x}Li_xCu_2O_3$ with the quasi-one-dimensional two-leg-ladder structure. We succeeded in extending the solubility limit of Li in $Mg_{1-x}Li_xCu_2O_3$ from $x = 0.12$ to $x = 0.60$ by using the high-pressure synthesis technique. The antiferromagnetic transition temperature rapidly decreases with increasing Li content from 94 K at $x = 0$ to 7.5 K at $x = 0.30$, and takes an almost constant value (3–6 K) at $x \geqslant 0.35$. The antiferromagnetic order still exists even at $x = 0.60$, where the formal valence of Cu is as large as +2.30. The temperature dependence of the specific heat suggests the finite contribution of the electronic specific heat at $x = 0.20$–0.60, which is consistent with high valence of Cu. Nevertheless, the temperature dependence of resistivity shows a variable range hopping behavior in the whole x ranges, and the insulating behavior survives under the pressure up to 2.9 GPa. This peculiar behavior is owing to the disorder originating from the intersite atom exchanges due to the similar ionic radius of cations in $Mg_{1-x}Li_xCu_2O_3$. Nonmagnetic ions of Mg^{2+} and Li^{+} are introduced into the Cu_2O_3 planes of $Mg_{1-x}Li_xCu_2O_3$, resulting in the localization of doped hole carriers.

DOI: 10.1103/PhysRevB.101.245112

I. INTRODUCTION

The discovery of cuprate superconductors with the high superconducting transition temperature (T_c) [1] had a great impact on condensed matter physics, and extensive research on these materials has been performed for over 30 years. These studies revealed that the parent compound with a common structural unit, CuO_2 plane, is an insulator driven by the strong electron-electron interaction (Mott insulator) and that the unconventional superconductivity emerges by carrier doping into the CuO_2 plane. Among various high-T_c cuprate superconductors, $Sr_{14-x}Ca_xCu_{24}O_{41}$ is known to be the only exceptional material not containing a CuO_2 plane. This material consists of a sum of a spin-1/2 two-leg ladder (Cu_2O_3 ladder) and a nonmagnetic chain (CuO_2 chain). The average valence of Cu in $Sr_{14}Cu_{24}O_{41}$ is +2.25; however, the temperature (T) dependence of resistivity shows an insulating behavior because hole carriers are localized at CuO_2 chain sites [2,3]. While the isovalent Ca^{2+} ion substitution for Sr^{2+} ion does not change the average valence of Cu, it leads to a charge transfer from the charge reservoir CuO_2 chains to Cu_2O_3 ladders, and reduces the resistivity remarkably [3]. Furthermore, the application of the physical pressure for $Sr_{14-x}Ca_xCu_{24}O_{41}$ with $x = 9$–13.6 induces superconductivity [2,4]. This superconductivity is considered to occur at Cu_2O_3 ladder planes, to which hole carriers are transferred from the CuO_2 chains by the application of pressures [2,3].

Iron-based superconductors [5] are another high-T_c superconductor family next to cuprates. Iron-based superconductors also have a common structural unit of iron square lattice in the FeX_4 tetrahedra layers (X = pnictogen and chalcogen [6,7]). However, there is an exceptional material $BaFe_2S_3$, which has a quasi-one-dimensional structure consisting of Fe ladders composed by edge-shared FeS_4 tetrahedra. This material is a Mott insulator and shows a stripe-type antiferromagnetic order below the antiferromagnetic transition temperature T_N of ~119 K. On applying pressure, a stripe-type antiferromagnetic order is suppressed, and then, a superconductivity with $T_c \sim 24$ K appears at pressures of 10–20 GPa [8,9].

Although both $Sr_{14-x}Ca_xCu_{24}O_{41}$ and $BaFe_2S_3$ exhibit the pressure-induced superconductivity on a pseudo-one-dimensional ladder structure, there are two clear differences among these two materials. One is the type of pressure-induced metal-insulator transition. The metal-insulator transition in $Sr_{14-x}Ca_xCu_{24}O_{41}$ is categorized into a filling-control-type Mott transition, and that in $BaFe_2S_3$ is categorized into a bandwidth-control-type one. The other difference is a relation between a magnetism and a superconductivity. There is no clear magnetic order around room pressure in $Sr_{14-x}Ca_xCu_{24}O_{41}$, which has a spin gap with ~500 K at $x = 0$ [10]. On the other hand, a superconducting phase is adjacent to a stripe-type antiferromagnetic phase in the pressure-temperature phase diagram of $BaFe_2S_3$. The material which bridges there two materials is useful for the better understanding of the superconductivity in the ladder lattice.

In this study we focus on ACu_2O_3 with the *Pmmn* (A = Mg and Ca) [11,12] and *Cmmm* (A = Sr) [13] space groups;

*imai@tohoku.ac.jp

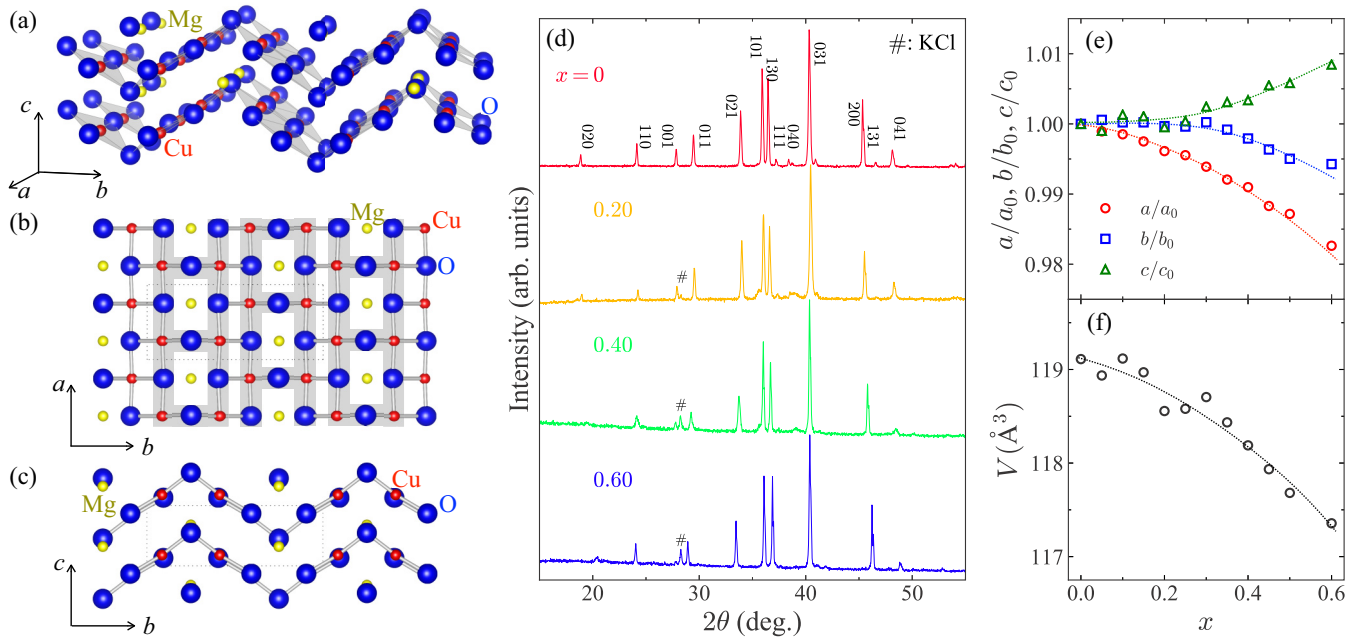

FIG. 1. Crystal structure of $MgCu_2O_3$ [(a) whole image, (b) the *ab* plane, and (c) the *bc* plane]. (d) X-ray diffraction patterns for polycrystals of $Mg_{1-x}Li_xCu_2O_3$ with $x = 0$, 0.20, 0.40, and 0.60. The Miller indexes on the basis of the orthorhombic *Pmmn* are also shown. The symbols # represent peaks attributed to KCl which is derived from the oxidizing agent $KClO_4$. Composition dependence of (e) lattice parameters (a, b, and c) normalized by the values of a, b, and c at $x = 0$ ($a_0 = 4.00$ Å, $b_0 = 9.34$ Å, and $c_0 = 3.19$ Å) and an unit cell volume (V) on the basis of the orthorhombic *Pmmn* space group in $Mg_{1-x}Li_xCu_2O_3$. The dotted curves in (e) and (f) are a guide for the eye.

the crystal structure of $MgCu_2O_3$ is shown in Figs. 1(a)–1(c). Comparing to $Sr_{14-x}Ca_xCu_{24}O_{41}$, ACu_2O_3 has a simple pseudo-one-dimensional structure with a Cu_2O_3 unit stacked via A^{2+} ions, and does not contain the CuO_2-chain structure. The material $SrCu_2O_3$ is the prototype of two-leg spin-ladder compounds, and both of the Cu-O-Cu bond angles along the leg and rung directions are 180°. On the other hand, as shown in shown in Figs. 1(b) and 1(c), $MgCu_2O_3$ and $CaCu_2O_3$ have buckled two-leg ladders, which are formed by the linear Cu-O-Cu bond along the leg direction (a axis) with the bond angle of 180° and the buckled Cu-O-Cu bond along the rung direction (b axis) with the bond angle of 105° ($A = $ Mg) and 123° ($A = $ Ca) [11,12]. The temperature dependence of magnetic susceptibility shows a broad peak in $A = $ Sr [14], which is the spin gap feature as in $Sr_{14-x}Ca_xCu_{24}O_{41}$ [15]. On the other hand, a clear kink resulting from the antiferromagnetic transition is observed at $T_N = 94$ K ($A = $ Mg) [16] and 24 K ($A = $ Ca) [17]. Below T_N, the magnetic structure of $MgCu_2O_3$ is revealed to be the stripe-type one [16], in which the spins are arranged ferromagnetically along the rung direction (b axis) and antiferromagnetically along the leg direction (a axis); this is consistent with the Goodenough-Kanamori rules [18,19]. In the antiferromagnetically ordered state, the spin is roughly pointing toward the rung direction (b axis). Hence, the magnetic structure of $MgCu_2O_3$ is similar to that of the Fe-based ladder superconductor $BaFe_2S_3$. On the other hand, the magnetic structure of $CaCu_2O_3$ is reported to be a spiral magnetic structure with spins rotating in the *ac* crystallographic plane [17]. In this way, $MgCu_2O_3$ and $CaCu_2O_3$ with a buckled two-leg ladder structure show an antiferromagnetic order unlike copper oxide with a flat two-leg ladder structure. Then, one question arises; does the carrier doping into the buckled ladder cuprates induce the metallic/superconducting state? Theoretically, an appearance of a superconductivity is predicted by doping hole carriers into ACu_2O_3 with a buckled ladder structure [20]. On the other hand, the atomic substitution in ACu_2O_3 is known to be very difficult. While the isovalent substitution such as $Mg_{1-x}Ca_xCu_2O_3$ [21,22] and $MgCu_{2-x}Zn_xO_3$ [23–25] were reported, there are few reports on the carrier doping into ACu_2O_3. One rare example of carrier-doping systems is the hole-doped one $Mg_{1-x}Li_xCu_2O_3$ [16,26,27]. The solvability limit of $Mg_{1-x}Li_xCu_2O_3$ synthesized by the solid state reaction was as small as $x = 0.12$. In this system, T_N decreases with increasing Li content from 94 K at $x = 0$ to 24 K at $x = 0.12$. Hence, the antiferromagnetic order was not completely suppressed by the Li substitution.

Here, motivated by a novel electronic state found in various ladder materials, we investigate the carrier-doping effect of $MgCu_2O_3$. By using a high-pressure synthesis, we successfully prepare $Mg_{1-x}Li_xCu_2O_3$ with a wide composition range $x = 0$–0.60. The electrical resistivity shows a gradual decrease on the carrier doping, indicating that mobile carriers are actually introduced into the system. However, the variable-range hopping-type temperature dependence persists in the wide x compositions, and does not show a metallic behavior. The antiferromagnetic transition temperature rapidly decreases on the hole doping, suggesting that introduced carriers destabilize the magnetically ordered state by cutting the superexchange interaction path. However, the antiferromagnetic order with $T_N \sim 3$ K is observed even at $x = 0.60$. The behaviors in the heavily hole-doped range are considered to be due to the atomic disorder, which is produced by the inter-site ion exchanges of Mg^{2+}, Li^+, and Cu^{2+} ions. Our

results highlight how $MgCu_2O_3$ resembles and differs from $Sr_{14-x}Ca_xCu_{24}O_{41}$ and $BaFe_2S_3$, and suggest a more suitable Cu-based ladder material for exploring a new superconductor.

II. EXPERIMENT

The parent material $MgCu_2O_3$ is prepared by a solid state reaction [28]. Mixed powders of starting materials, MgO and CuO, with the prescribed molar ratio of 2 : 5 were pelletized and heated at 950 °C for 24 h in air. The Li-substituted polycrystalline samples $Mg_{1-x}Li_xCu_2O_3$ ($x = 0$–0.60) are synthesized by using a cubic-anvil-type high-pressure apparatus. We use two kinds of starting materials depending on the composition: one is MgO, CuO, Li_2CuO_2, and $KClO_4$ with a molar ratio of $(1-x) : (2-x/2) : x/2 : x/8$ for $x = 0$–0.25; the other is MgO, CuO, Li_2O, and $KClO_4$ with a molar ratio of $(1-x) : 2 : x/2 : x/8$ for $x = 0.15$, 0.30–0.60. Here $KClO_4$ is used as an oxidizing agent. For obtaining highly Li-doped samples, it is a crucial importance to use Li_2O as a Li source. Mixed starting materials are placed in a gold capsule and are loaded into a pyrophyllite cube. These are heated at ~800 °C for 30 min at ~4 GPa. All the products are characterized by the powder x-ray diffraction (XRD) using the Cu $K\alpha$ radiation at room temperature. The electrical resistivity ρ was measured by the four-terminal method over the temperature range of 4.2 to 300 K. The resistivity measurements at high pressure up to 2.9 GPa are performed by using a hybrid piston cylinder-type high-pressure cell made of CuBe and NiCrAl alloys [29]. The pressure medium is Daphne 7373 (Idemitsu Kosan), and the pressure is determined by the ruby fluorescence method at room temperature [30]. Magnetic susceptibility χ measurements are performed using a superconducting quantum interference device (SQUID) magnetometer. The specific heat C is measured by the thermal-relaxation method at temperatures as low as 2 K under a magnetic field of $\mu_0 H = 0$–9 T with a use of a commercial apparatus (Physical Property Measurement System, Quantum Design).

III. RESULTS

Figure 1(d) shows the XRD patterns for polycrystalline samples of $Mg_{1-x}Li_xCu_2O_3$ with $x = 0$–0.60. Except for peaks attributed to KCl originating from the oxidizing agent $KClO_4$, all peaks can be indexed on the basis of a orthorhombic space group of *Pmmn* [11], indicating the formation of a single phase. The 2θ values of 200 peaks increase with increasing x in a continuous manner, which indicates that the Li atoms are systematically substituted into the materials. The experimentally determined lattice parameters and the unit cell volume are plotted as a function of x in Figs. 1(e) and 1(f). With increasing x, the a and b values decreases, whereas the c value increases. As a result, the unit cell volume decreases with increasing x. The reduction of the a and b values correspond to the decrease in the Cu-O bond length due to the hole doping into the system. From the formation of a single-phase sample and the systematic change of lattice parameters, we conclude that the actual Li content is nearly identical to the nominal one; hereafter we use the nominal Li content x as the compositions of resultant samples $Mg_{1-x}Li_xCu_2O_3$. It should be noted that the solubility limit of Li greatly expands from 0.12 to 0.60. The high-pressure synthesis is effective for an expansion of solubility limit in this system.

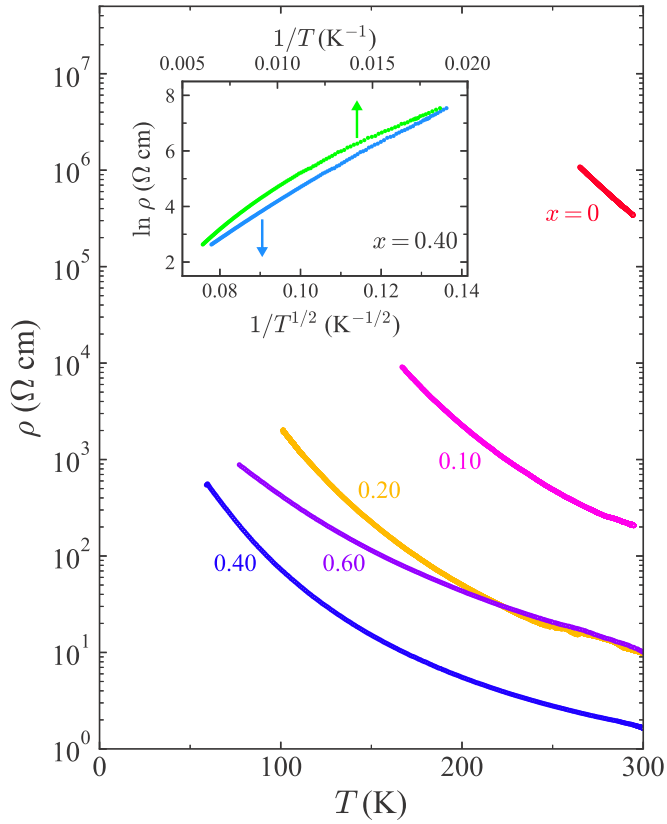

FIG. 2. Temperature (T) dependence of the resistivity (ρ) for $Mg_{1-x}Li_xCu_2O_3$ with $x = 0$, 0.10, 0.20, 0.40, and 0.60. The inset shows the same data plotted against $T^{-1/2}$ and T^{-1} for $x = 0.40$. The plotted temperature range is 50–200 K.

Figure 2 shows the temperature dependence of ρ for $Mg_{1-x}Li_xCu_2O_3$ with $x = 0$–0.60 at ambient pressure. The resistivity of the parent material $MgCu_2O_3$ with the divalent Cu ions is as large as $\sim 10^6$ Ω cm, and can only be measured around room temperature. Electrical resistivity decreases dramatically with increasing x, and ρ for $x = 0.60$ at room temperature is ~5 orders of magnitude smaller than that of $MgCu_2O_3$. This drastic decrease of ρ is owing to an introduction of hole carriers into the samples. Although the formal valence of Cu reaches as large as +2.30 at $x = 0.60$, which corresponds to 0.30 holes/Cu, all the samples investigated in this study do not show a metallic behavior. One of the possible reasons for the localized behavior is the oxygen vacancy. However, it would not be in our case; we adopt the high-pressure synthesis method by using $KClO_4$ as an oxidizing agent, which prevents the deviation of oxygen content from the stoichiometric value. If there are any oxygen vacancies in the resultant samples, the peaks originating from KO_2 must appear in x-ray diffraction patterns. In Fig. 1(d), however, there are no peaks coming from KO_2, which is the strong evidence of negligible oxygen vacancy in our sample. We estimate the activation energy E_g from the fitting of ρ with a equation $\rho = \rho_0 \exp(E_g/2k_BT)$, where ρ_0 is the pre-exponential factor, and k_B is the Boltzmann constant. Then,

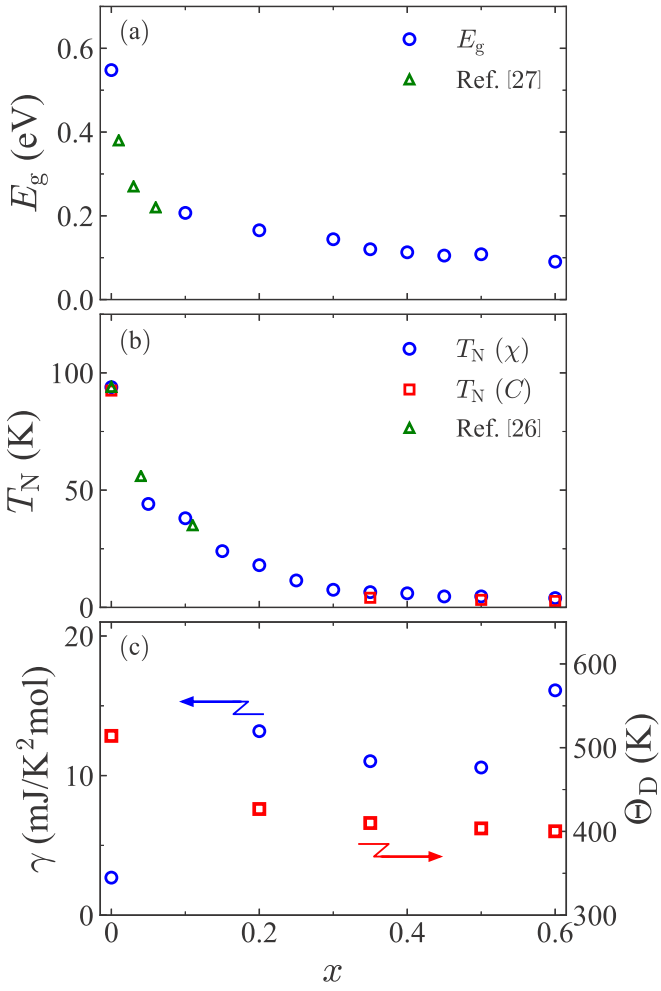

FIG. 3. Composition dependencies of (a) the activation energy (E_g) estimated from the resistivity, (b) the antiferromagnetic transition temperature (T_N), and (c) the electronic specific heat coefficient (γ) and the Debye temperature (Θ_D) for $Mg_{1-x}Li_xCu_2O_3$ with (x = 0–0.60). The T_N values are determined by the magnetic susceptibility (blue circle) and specific heat (red square). For comparison, previously reported values of E_g and T_N are also plotted in (a) and (b) as green triangles [26,27]. The dotted curves in (c) are a guide for the eye.

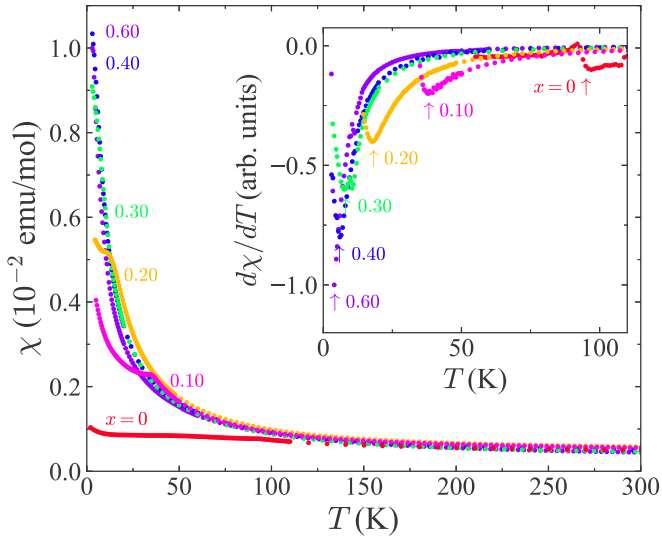

FIG. 4. Temperature (T) dependencies of the magnetic susceptibility (χ) for $Mg_{1-x}Li_xCu_2O_3$ with $x = 0$, 0.10, 0.20, 0.30, 0.40, and 0.60 at a magnetic field of $\mu_0 H = 1$ T. The inset shows the temperature differentials of χ ($d\chi/dT$). The arrows indicate the antiferromagnetic transition temperature.

obtained values are plotted in Fig. 3(a) and are consistent with the previously reported values at $x = 0.01$–0.09 [27]. With increasing x, E_g decreases dramatically for $x = 0$–0.30, while it is almost constant for $x = 0.35$–0.60.

Figure 4 shows the temperature dependence of χ for $Mg_{1-x}Li_xCu_2O_3$ with $x = 0$–0.60 under the magnetic field of $\mu_0 H = 1$ T. The χ-T curves show kink anomalies at low temperatures; this can be clearly observed as a dip structure in the temperature derivative of χ shown in the inset of Fig. 4. These anomalies are considered to be owing to the formation of the stripe-type antiferromagnetic order [16,28]. We define the temperature at which $d\chi/dT$ takes its local minimum as the antiferromagnetic transition temperature T_N, which is plotted as a function of x in Fig. 3(b). At $x = 0$–0.30, the T_N value rapidly decreases from 93.9 K at $x = 0$ to 7.5 K at $x = 0.30$ with increasing x. The T_N value at $x = 0$ is consistent with the previously reported value [26]. However, on further increasing x up to 0.60, the T_N value shows little change and becomes as small as 4.0 K at $x = 0.60$. This indicates the robust antiferromagnetic state against further introduction of hole carriers. This dramatic/subtle change in T_N at $x = 0$–$0.30/0.35$–0.6 is similar to the trend observed in the composition dependence of E_g.

The specific heat divided by the temperature C/T under zero magnetic field is plotted as a function of T^2 in Fig. 5. The specific heat for $x = 0$ has a broad peak structure at 93 K (inset of Fig. 5), which is attributable to the antiferromagnetic transition. The entropy release across the transition is roughly estimated to be 90–120 mJ/(Cu mol K) after subtracting the lattice specific heat. This value is quite small compared with the expected total magnetic entropy for $S = 1/2$ spins, $N_A k_B \ln(2S + 1) \approx 5.76$ J/(Cu mol K), where N_A is the Avogadro number. Such discrepancy is frequently observed in a low-dimensional spin system, in which the magnetic order develops in a wide temperature range owing to large quantum fluctuations. On substitution Li atoms, the peak temperature is smoothly lowered, and becomes 3.2 K at $x = 0.50$. We define the temperature at which C/T takes its local maximum to be T_N, which is plotted as a function of x in Fig. 3(b), being in good agreement with T_N deduced from the magnetic susceptibility. We then performed the specific heat measurements under the magnetic field of $\mu_0 H = 9$ T for $x = 0.50$ (Fig. 5). The peak structure at 3.2 K is suppressed by the application of the magnetic field, which is caused by the suppression of the antiferromagnetic order by the magnetic field. We note that there is almost no impact of the magnetic field on C above 20 K, indicating that the magnetic contribution becomes very small in this temperature range.

In order to separate the electron and phonon contributions in C, we fitted the specific heat data at low temperatures to the expression $C = \gamma T + \beta T^3$, where the γ and β terms

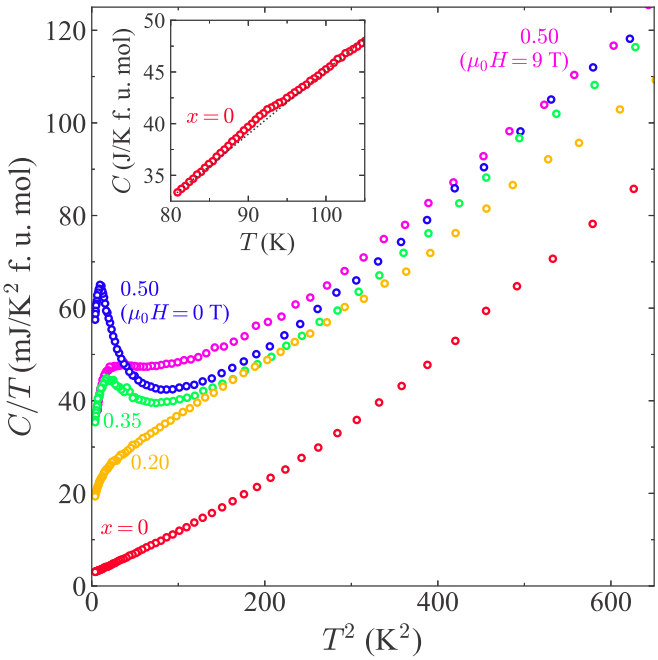

FIG. 5. Specific heat divided by the temperature (C/T) plotted against T^2 for $Mg_{1-x}Li_xCu_2O_3$ with $x = 0$, 0.20, 0.35, and 0.50 under zero magnetic field. For $x = 0.50$, the data under a magnetic field of $\mu_0 H = 9$ T are also plotted. The inset is an enlarged plot of C around the antiferromagnetic transition temperature for $x = 0$. The dotted curve in the inset corresponds to the contributions of phonons.

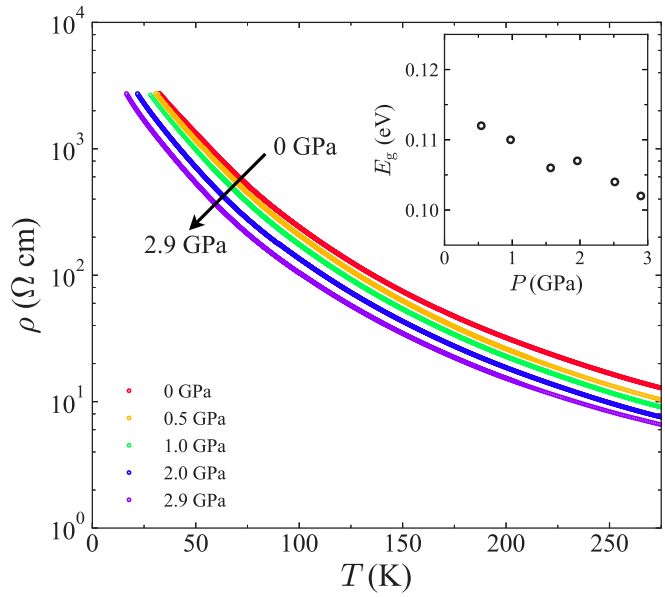

FIG. 6. Temperature (T) dependencies of the resistivity (ρ) for $Mg_{1-x}Li_xCu_2O_3$ with $x = 0.60$ under high pressures of 0, 0.5, 1.0, 2.0, and 2.9 GPa. The inset shows the pressure (P) dependence of the activation energy E_g.

correspond to the electron and phonon contributions, respectively. Here the fitted temperature range is set to be 2–6 K for $x = 0$ and 20–23 K for $x = 0.20$–0.60, which permits us to ignore the magnetic contributions. The obtained γ values are shown in Fig. 3(c). For $x = 0$, the contribution of electron specific heat is hardly seen, which is consistent with a Mott insulating state in $MgCu_2O_3$. However, the finite values of γ are observed at $x = 0.20$–0.60, although these samples show an insulating behavior in ρ; the reason will be discussed later. The γ value at $x = 0.20$ is slightly large from the interpolated value from the composition dependence, because it includes some magnetic contribution in addition to the electronic contribution owing to the closeness of $T_N \sim 18$ K and the fitting temperature range. As can be seen in Fig. 3(c), the γ values show a modest composition dependence at $x = 0.35$–0.60; this trend is similar to those seen in E_g and T_N. Concerning phonon contributions, we deduce the Debye temperature Θ_D by using the formula $\beta = 12\pi^4 NR/5\Theta_D^3$ where N is the number of atoms in a formula unit ($N = 6$) and R is the gas constant. The obtained values are plotted against x in Fig. 3(c). With increasing x, Θ_D decreases from 514 K at $x = 0$ to 400–410 K at $x = 0.35$–0.60. This composition dependence is anomalous in the light of the simple expectation based on the atomic mass. We speculate that the observed x dependence is owing to weakening in a interatomic bond strength among the Cu_2O_3 units.

The application of pressure is an effective method to metalize the Mott insulator. We here choose the heavily hole-doped compound $Mg_{1-x}Li_xCu_2O_3$ with $x = 0.60$, and investigate the pressure effect. Figure 6 represents the temperature dependence of ρ under high pressures up to 2.9 GPa. The resistivity monotonically decreases with increasing pressure; however, the impact of pressure is rather small, and the system does not show a metallic behavior even at 2.9 GPa. This behavior is in a sharp contrast to the appearance of pressure-induced metallic state accompanied by the superconducting transition around 3.5 GPa in $Sr_{0.4}Ca_{13.6}Cu_{14}O_{41}$ [4]. The activation energy E_g is plotted in the inset of Fig. 6. The extrapolation of the data toward higher pressure tells us that at least 30 GPa is required to suppress the charge gap of this material.

IV. DISCUSSION

We now discuss electronic states in $Mg_{1-x}Li_xCu_2O_3$ with $x = 0$–0.60 on the basis of the x dependence of the physical quantities shown in Fig. 3. The charge gap rapidly decreases with increasing x at $x = 0$–0.30, in which the antiferromagnetic order is suppressed steeply. On the other hand, the charge gap takes an almost constant value at $x = 0.35$–0.60, where the stability of the antiferromagnetic order does not change considerably. We note here that the hole-doping level is as large as 0.30/Cu site at $x = 0.60$, which is expected to be enough to metalize the system. The observed behavior is in a stark contrast to the two-dimensional cuprate superconductors, in which a hole doping as small as 0.05/Cu site renders the system from the Mott insulator to a metal and destroys the long-range antiferromagnetic order. Here one might think a possibility that the copper valence is modified by the possible Li and O vacancies. However, this is unlikely since there are no impurity peaks in XRD patterns. In addition, the lattice parameter shows a systematic change as a function of Li content. These facts indicate that there are few deviations

of compositions from the nominal ones, and that the copper valence is +2.30 at $x = 0.60$.

One clue to understand the nature of the insulating state at $x = 0.35$–0.60 is gained from the specific heat measurements, which indicates a large electronic contribution of $\gamma \approx 10.6$–16.1 mJ/K^2 mol for $x = 0.35$–0.60. One can then conclude that the seeming insulating state at $x = 0.35$–0.60 actually has a finite density of states at the Fermi energy. Hence, one plausible candidate of the electronic state at $x = 0.35$–0.60 is an Anderson insulator [31–33]. To test such a possibility, we plot $\ln \rho$ for $x = 0.35$ against T^{-1} and $T^{-1/2}$ in the inset of Fig. 2. One can see that ρ obeys the $\rho \propto \exp(T^{-1/2})$ law over a temperature range of 60–180 K. These are the characteristics of the variable-range-hopping (VRH) process in the strong localization region in one dimension. Thus, $Mg_{1-x}Li_xCu_2O_3$ is considered to be a strongly localized system, where one-dimensional VRH-type behavior is realized. We conclude that this is the origin of the insulating state with a finite γ value in $Mg_{1-x}Li_xCu_2O_3$.

This strong localization effect is considered to be owing to the disorder effect among atomic sites on the low-dimensional crystal structure. The three cations, Mg^{2+}, Li^+, and Cu^{2+} ions, in $Mg_{1-x}Li_xCu_2O_3$, have a similar ionic radius, which cause a disorder in the atomic site. In other words, Cu^{2+} ions likely exist at the Mg/Li site, and Mg^{2+} and Li^+ ions likely exist at the Cu site. In fact, it has been reported from a neutron diffraction for $Mg_{1-x}Li_xCu_2O_3$ with $x = 0.12$ that Cu atoms occupy 12 % of the Mg site and that a small amount of Mg exists at the Cu site [26]. We also note that the intersite mixing between Cu and Li atoms has been reported for various inorganic materials [34,35]. Therefore, the Cu_2O_3 ladder plane in $Mg_{1-x}Li_xCu_2O_3$ is disturbed by nonmagnetic ions such as Li^+ and Mg^{2+}, and as a result, doped hole carriers are localized, preventing the appearance of metallic behavior. Because the one dimensionality of the Cu_2O_3 unit is strong in $Mg_{1-x}Li_xCu_2O_3$ with the buckled ladder plane (the Cu-O-Cu angle of the rung direction is 105°), the influence of the disorder on transport properties is more prominent in comparison with two-leg ladder cuprates with a flat ladder planes (the Cu-O-Cu angle of the rung direction is 180°).

On the other hand, we believe that the disorder also affects the spin state below T_N at $x = 0.35$–0.60, where T_N takes an almost constant value of ∼3–6 K. With increasing Li content, not only a hole concentration but also an atomic disorder increases, because the ionic radius of Li^+ is closer to that of Cu^{2+} than that of Mg^{2+}. At small hole concentration regime ($x = 0$–0.1), the former is more pronounced and the copper spin correlation sharply decreases with increasing hole concentrations. With further increasing hole concentration, the latter effect cannot be neglected, and the disorder permits the existence of short-range antiferromagnetic-ordered state even at highly hole-doped region. Indeed, we observe the spin-glass-like behavior at $x = 0.35$, that is, a irreversibility between zero-field-cooling and field-cooling processes in the magnetic susceptibility measurements under a low magnetic field (data not shown). The antiferromagnetic order at $x = 0$ seems to change into a spin-glass-like state around $x \approx 0.35$.

Finally, we briefly comment on how to improve the sample quality of carrier-doped ACu_2O_3. We had expected that $Mg_{1-x}Li_xCu_2O_3$ shows a metallic and superconducting behavior. However, owing to the atomic disorder, the carriers in the Cu_2O_3 plane of $Mg_{1-x}Li_xCu_2O_3$ are localized, and the spin state seems to be a glassy one. Therefore, for investigating the intrinsic properties on pure Cu_2O_3 plane in ACu_2O_3, it is necessary to remove the chemical disorder. Generally, the post-annealing process is effective for reducing a disorder. However, $Mg_{1-x}Li_xCu_2O_3$ with $x = 0.12$–0.60 is prepared only by a synthesis under high pressure, and thus samples are decomposed by the post-annealing process at ambient pressure; hence it is hard to improve sample quality by the annealing procedure in $Mg_{1-x}Li_xCu_2O_3$. Instead, it is more plausible to focus on $CaCu_2O_3$ material. Considering that the ionic radius of Ca^{2+} ion is much larger than that of Cu^{2+} ion, one can expect a small intersite exchange in $CaCu_2O_3$. Hence, it is highly expected to dope carriers into $CaCu_2O_3$ by the chemical substitution using the high-pressure synthesis technique. If such system is developed, one can straightforwardly compare electronic states with those of $Sr_{14-x}Ca_xCu_{24}O_{41}$ and $BaFe_2S_3$, and reach a better understanding of the electronic states in the buckled-ladder copper oxides.

V. SUMMARY

In summary, we prepare heavily hole-doped cuprates $Mg_{1-x}Li_xCu_2O_3$ with the quasi-one-dimensional two-leg-ladder structure and investigate their electronic properties. We succeeded in extending the solubility limit of Li in $Mg_{1-x}Li_xCu_2O_3$ from $x = 0.12$ to $x = 0.60$ by using a high-pressure synthesis technique. The charge gap and the antiferromagnetic transition temperature rapidly decreases with increasing Li content for $x = 0$–0.30, indicating that mobile carriers are introduced into the system. However, the charge gap takes an almost constant value for $x = 0.35$–0.60, keeping an insulating state in all the composition range investigated here. The insulating state is robust under pressures up to 2.9 GPa. The antiferromagnetic order is still observed around ∼3 K even at $x = 0.60$, where the formal valence of Cu is as large as +2.30. The temperature dependence of the specific heat suggests the finite contribution of the electronic specific heat at $x = 0.20$–0.60, which seemingly contradicts the insulating behaviors in the electrical resistivity. This peculiar behavior in the heavily substituted range is originating from the disorder produced by the intersite atomic exchange of nonmagnetic Mg^{2+}/Li^+ ions and magnetic Cu^{2+} ions, which results in the the localization of doped hole carriers.

ACKNOWLEDGMENTS

This work was performed under the Inter-university Cooperative Research Program of the Institute for Materials Research, Tohoku University (Proposals No. 18K0201 and No. 19K0202). This work was supported by JSPS KAKENHI Grants No. JP18H01159, No. JP18H04302, No. JP18K03531, No. JP19H04685, No. JP19H05822, No. JP19H05823, and No. JP19K21837. This work was also supported by JST CREST Grant No. JP19198318, Japan.

[1] J. G. Bednorz and K. A. Müller, Z. Phys. B **64**, 189 (1986).
[2] N. Motoyama, H. Eisaki, S. Uchida, N. Takeshita, N. Môri, T. Nakanishi, and H. Takahashi, Europhys. Lett. **58**, 758 (2002).
[3] T. Osafune, N. Motoyama, H. Eisaki, and S. Uchida, Phys. Rev. Lett. **78**, 1980 (1997).
[4] M. Uehara, T. Nagata, J. Akimitsu, H. Takahashi, N. Môri, and K. Kinoshita, J. Phys. Soc. Jpn. **65**, 2764 (1996).
[5] Y. Kamihara, T. Watanabe, M. Hirano, and H. Hosono, J. Am. Chem. Soc. **130**, 3296 (2008).
[6] H. Hosono and K. Kuroki, Physica C **514**, 399 (2015).
[7] Y. Imai, F. Nabeshima, and A. Maeda, Condens. Matter **2**, 25 (2017).
[8] H. Takahashi, A. Sugimoto, Y. Nambu, T. Yamauchi, Y. Hirata, T. Kawakami, M. Avdeev, K. Matsubayashi, F. Du, C. Kawashima, H. Soeda, S. Nakano, Y. Uwatoko, Y. Ueda, T. J. Sato, and K. Ohgushi, Nat. Mater. **14**, 1008 (2015).
[9] T. Yamauchi, Y. Hirata, Y. Ueda, and K. Ohgushi, Phys. Rev. Lett. **115**, 246402 (2015).
[10] S. Tsuji, K. Kumagai, M. Kato, and Y. Koike, J. Phys. Soc. Jpn. **65**, 3474 (1996).
[11] H. Drenkhahn and H. Müller-Buschbaum, Z. Anorg. Allg. Chem. **418**, 116 (1975).
[12] C. L. Teske and H. Müller-Buschbaum, Z. Anorg. Allg. Chem. **370**, 134 (1969).
[13] Z. Hiroi, M. Azuma, M. Takano, and Y. Bando, J. Solid State Chem. **95**, 230 (1991).
[14] M. Azuma, Z. Hiroi, M. Takano, K. Ishida, and Y. Kitaoka, Phys. Rev. Lett. **73**, 3463 (1994).
[15] N. Motoyama, T. Osafune, T. Kakeshita, H. Eisaki, and S. Uchida, Phys. Rev. B **55**, R3386 (1997).
[16] M. Winkelmann, H. A. Graf, and N. H. Andersen, Phys. Rev. B **49**, 310 (1994).
[17] V. Kiryukhin, Y. J. Kim, K. J. Thomas, F. C. Chou, R. W. Erwin, Q. Huang, M. A. Kastner, and R. J. Birgeneau, Phys. Rev. B **63**, 144418 (2001).
[18] J. B. Goodenough, *Magnetism and Chemical Bond* (Krieger, New York, 1976).
[19] J. Kanamori, J. Phys. Chem. Solids **10**, 87 (1959).
[20] N. Plakida, A. Vladimirov, and S.-L. Drechsler, Physica C: Superconductivity **408-410**, 232 (2004).
[21] N. Kobayashi, Z. Hiroi, and M. Takano, J. Solid State Chem. **132**, 274 (1997).
[22] K. Ruck, W. Pitschke, G. Krabbes, M. Wolf, D. Eckert, and K.-H. Müller, J. Phys. Chem. Solids **63**, 1901 (2002).
[23] Q. Zhou, H. Suzuki, and T. Yamadaya, J. Low Temp. Phys. **115**, 229 (1999).
[24] C. Sekar, G. Krabbes, A. Teresiak, M. Wolf, D. Eckert, and K.-H. Müller, J. Cryst. Growth **275**, e1961 (2005).
[25] M. Azuma, Y. Fujishiro, M. Takano, M. Nohara, and H. Takagi, Phys. Rev. B **55**, R8658 (1997).
[26] M. Winkelmann, H. Graf, N. Andersen, T. Zeiske, and D. Hohlwein, J. Mag. Mag. Mater. **104-107**, 871 (1992).
[27] Y. Tsuchiya and K. Oh-ishi, J. Solid State Chem. **168**, 85 (2002).
[28] T. Zeiske, H. Graf, H. Dachs, and K. Clausen, Solid State Commun. **71**, 501 (1989).
[29] Y. Uwatoko, S. Todo, K. Ueda, A. Uchida, M. Kosaka, N. Mori, and T. Matsumoto, J. Phys.: Condens. Matter **14**, 11291 (2002).
[30] G. J. Piermarini, S. Block, J. D. Barnett, and R. A. Forman, J. Appl. Phys. **46**, 2774 (1975).
[31] P. W. Anderson, Phys. Rev. **109**, 1492 (1958).
[32] S. Marnieros, L. Bergé, A. Juillard, and L. Dumoulin, Physica B: Condens. Matter **259-261**, 862 (1999).
[33] T. Ying, Y. Gu, X. Chen, X. Wang, S. Jin, L. Zhao, W. Zhang, and X. Chen, Sci. Adv. **2**, e1501283 (2016).
[34] R. R. Heikes and W. D. Johnston, J. Chem. Phys. **26**, 582 (1957).
[35] J. Bobroff, W. A. MacFarlane, H. Alloul, P. Mendels, N. Blanchard, G. Collin, and J.-F. Marucco, Phys. Rev. Lett. **83**, 4381 (1999).